

# A Biological Gear in the Human Middle Ear

Hongxue Cai, Ryan P. Jackson, Charles Steele and Sunil Puria\*

Otobiomechanics group, Stanford University

\*Corresponding author: 496 Lomita Mall, Stanford, CA 94305, puria@stanford.edu

**Abstract:** A three-dimensional (3D) finite element (FE) model was developed to simulate the motion modes of the human middle ear structures. The model was based entirely on 3D reconstruction obtained from micro Computed Tomography (microCT) imaging. We solve the acoustics-structure interaction problem using COMSOL Multiphysics. Our results show that at low frequencies, the classical hinging motion is dominant, as expected. However, at high frequencies, we observe multi-resonance vibration modes at the eardrum and a biological bevel-gear like response at the malleus-incus complex. This suggests that the middle ear motion modes and dynamics are determined by the special anatomical features (saddle shape of the MIJ, asymmetry of the eardrum, and cylindrical malleus shape in larger mammals) and the three-dimensional inertial properties of the ossicles, and the twisting mode of the malleus and incus are required in larger mammals, like humans, in order to reduce the inertia due to ossicle mass.

**Keywords:** Human middle ear, Finite element analysis, Acoustic-structure interaction, Malleus-incus joint, Temporal bone.

## 1. Introduction

Mammals are unique among vertebrates in their ability to hear high-frequency sounds. To support high frequency transmission, the mammalian middle ear (ME) construction is unique. It transfers acoustic energy from the low-density air of the external ear canal (EC) to the high-density fluid of the inner ear (Bekesy, 1960; Wever and Lawrence, 1950). The middle ear bones are connected through two mobile joints, the malleus-incus joint (MIJ) and the incudostapedial joint (ISJ). These synovial joints, consisting of joint capsule and synovial fluid inside, play an important role in sound transmission. However, due to the shape-complexity and extremely small size, most existing middle ear finite-element (FE) analyses model the MIJ and ISJ as fused joints and make

inaccurate assumptions regarding anatomy (Homma *et al.*, 2009; Wada and Metoki, 1992). O'Connor and Puria (2008) developed a circuit model for the human middle ear which was shown to be in closer agreement with physiological measurements than previous lumped-element models (Feng and Gan, 2004; Godde *et al.* 1994; Kringlebotn, 1988). However, such lumped-parameter models, with detailed ME complex geometry and material compositions ignored, are unable to answer some structure-related questions such as the hypothesized existence of the bevel-gear mechanism at the MIJ complex at high frequencies (Puria and Steele, 2010). Gan *et al.* (2004) included the external ear canal (EC), tympanic membrane (eardrum), ossicular bones, middle ear suspensory ligaments/muscles, and ME cavity in their FE model, but did not report detailed motion patterns at the MIJ complex.

The purpose of this research is to develop a 3D FE model using accurate anatomical data to simulate the motion modes of human ME structures. We found a twisting motion at the MIJ complex at high frequencies, a biological gear in the human middle ear.

## 2. Method

We developed our current FE model using COMSOL that allows us to loft 2D geometric objects to construct complex 3D structures. The model geometry, including the ear canal, tympanic membrane (eardrum), ossicular bones (malleus, incus and stapes), suspensory soft attachments and middle ear joints, was based entirely on 3D reconstruction (Fig. 1) obtained from micro Computed Tomography (microCT) imaging (Sim and Puria, 2008). A set of section images of the ME complex, segmented in AMIRA software platform (Visage Imaging, Inc., San Diego, CA), were digitized by our costumer-developed software to construct COMSOL 2D geometric objects which were further lofted to build the 3D geometry of the ME. FE mesh was generated by COMSOL mesh

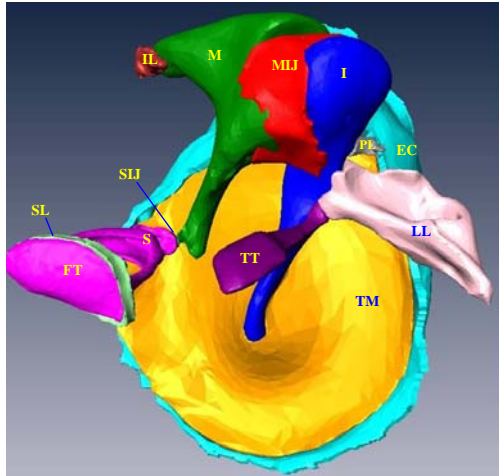


**Figure 1.** 3D reconstruction of a left human middle ear with partial external ear canal. M - malleus; I - incus; S - stapes; MIJ - malleus-incus joint; SIJ - incudostapedial joint; FT - footplate of the stapes; TM - tympani membrane (eardrum); EC - ear canal; TT - tensor tympani tendon; LL - lateral ligament of the malleus; PL - posterior ligament of the malleus; IL - incus ligament; SL - stapes annular ligament.

generator. Figure 2 shows the model mesh of a human left ear including the EC, tympani membrane (eardrum), MIJ, SIJ, and ME ossicles with soft attachments including tensor tympani tendon (TT) of the malleus, incus ligament (IL) and stapedius annular ligament (SL). The ME cavity was not modeled in this study. Structures were meshed by four-noded tetrahedrons with a total of 94013 elements. Note that the MIJ and SIJ were modeled as fluid-filled mobile joints by assigning to them complex-valued Young's modulus. The input of the model is a 80dB sine pressure wave at the entrance of the ear canal. Boundary conditions include fix end of the TT, LL, PL and IL, zero displacement at the outer surface of the SL and EC, as well as at the edge of the eardrum. The cochlea was modeled as an equivalent mechanical load based on the effective resistance value of 30 G $\Omega$  reported by Aibara *et al.* (2001), and the mass and stiffness of the cochlear fluid are assumed to be insignificant (Puria and Allen 1991; Shera and Zweig 1991).

The material properties of various components were initially obtained from the literature (Fay *et al.*, 2006; Sim *et al.*, 2007), including past studies of FE middle-ear modeling (Koike *et al.*, 2002; Gan *et al.*, 2004; Homma *et al.*, 2009), and tuned to produce overall magnitude and phase agreement with ear canal pressure ( $P_{EC}$ ) to stapes velocity ( $V_{st}$ ) transfer function ( $V_{st}/P_{EC}$ ) measurements (Fig. 3) as well as with the velocity ratio ( $V_{st}/V_{um}$ ) data between the umbo and stapes footplate (Fig. 4). Table I shows the final material property values of the middle-ear components used in the present model.

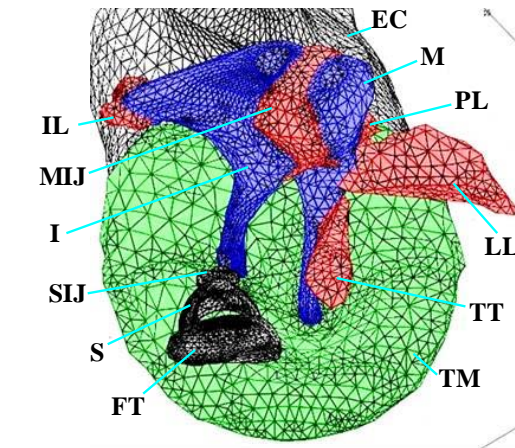


**Figure 2.** Model mesh of a left human middle-ear structures with external ear canal (EC in black). Please see Figure 1's caption for a complete list of abbreviations. FE meshes are four-noded tetrahedrons with a total of 94013 elements. The ME cavity is not included in the model.

All frequency-response acoustics-structure interaction responses were calculated using COMSOL Multiphysics solvers.

**3. Results**

### 3.1 Validation of the FE model

#### 3.1 Validation of the FE model

Figure 3 shows the comparison of EC pressure to stapes velocity transfer function ( $V_{st}/P_{EC}$ ) between published experimental measurements (symbols) and model curves (lines). The  $V_{st}/P_{EC}$  experimental data were made on 16 ears, including seven living ears measured by Huber *et al.* (2001) (square markers), for which, magnitude adjustments were made by Chien *et al.* (2006) on frequencies below approximately 2kHz to account for possible methodological differences between living ear and temporal bone

ear studies (O'Connor and Puria, 2008). The stapes-footplate velocity was projected to the piston-like direction i.e., the direction perpendicular to the footplate. For comparison,  $V_{st}/P_{EC}$  model curves from other studies are also shown in Fig. 3 (thin dash lines): O'Connor and Puria, 2008 (red); Kringlebotn, 1988 (cyan); Goode *et al.*, 1994 (magenta); and Feng and Gan, 2004 (black). Our FE model fit were plotted in blue thick lines. Both the magnitude (upper plot) and phase (lower plot) exhibit reasonably agreement with the measurements.

**Table 1:** Material properties used in the FE model

Material property	Value	Unit
Malleus:		
Young's modulus	$14 \times 10^9$	Pa
Density	3590	$\text{kg/m}^3$
Incus:		
Young's modulus	$14 \times 10^9$	Pa
Density	3230	$\text{kg/m}^3$
Stapes:		
Young's modulus	$14 \times 10^9$	Pa
Density	2200	$\text{kg/m}^3$
MIJ:		
Young's modulus	$6 \times 10^6 \times A^*$	Pa
Density	3200	$\text{kg/m}^3$
SIJ:		
Young's modulus	$6 \times 10^6 \times A$	Pa
Density	1200	$\text{kg/m}^3$
Eardrum:		
Young's modulus	$1 \times 10^7 \times A$	Pa
Density	1200	$\text{kg/m}^3$
TT, LL, PL, IL:		
Young's modulus	$1 \times 10^6 \times A$	Pa
Density	1100	$\text{kg/m}^3$
SL:		
Young's modulus	$1 \times 10^5 \times A$	Pa
Density	1100	$\text{kg/m}^3$
Air:		
Speed	343	m/s
Density	1.29	$\text{kg/m}^3$
Poisson's ratio	0.47	
Cochlear load	$30 \times 10^9$	$\text{G}\Omega$

\*Note:  $A = (1 + i \times 0.1 \times f / 1000)$ , with  $i = \sqrt{-1}$ , and  $f$  is the simulation frequency.

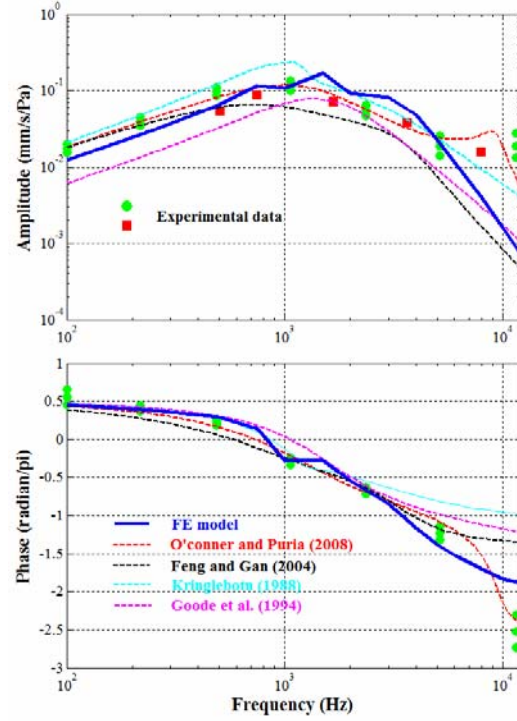
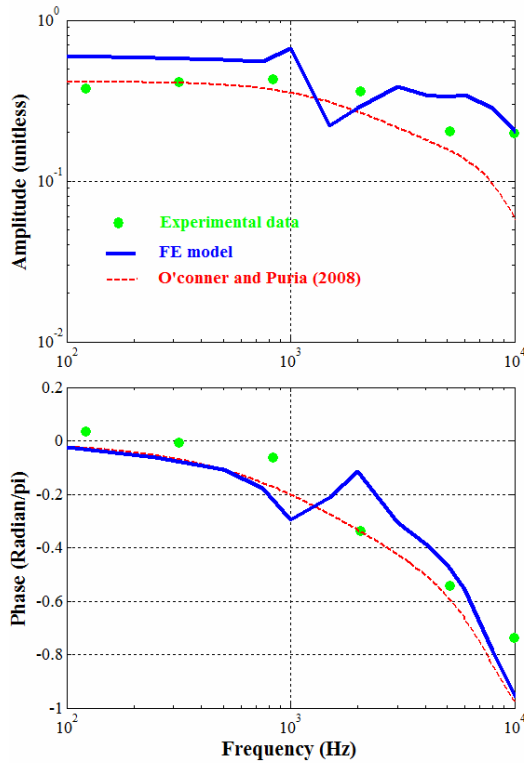


**Figure 3.** Model  $V_{st}/P_{EC}$  curves compared to the corresponding measured curves. The  $V_{st}/P_{EC}$  measurements are shown in symbols (circles and squares). The upper plot contains magnitude curves in units of  $(\text{mm/s})/\text{Pa}$ , while the lower plot contains the phase curves in units of  $\text{radian}/\pi$ . Our model fit was plotted in thick blue line, while simulation curves from previous models are shown in thin dash lines.

Figure 4 compares our simulation of the velocity ratio ( $V_{st}/V_{um}$ ) between the umbo and stapes footplate to those measured by Aibara *et al.* (2001). Red thin dash lines are model curves from O'Connor and Puria (2008). Again, both the amplitude (upper plot) and phase (lower plot) of our FE model closely match the experimental data.

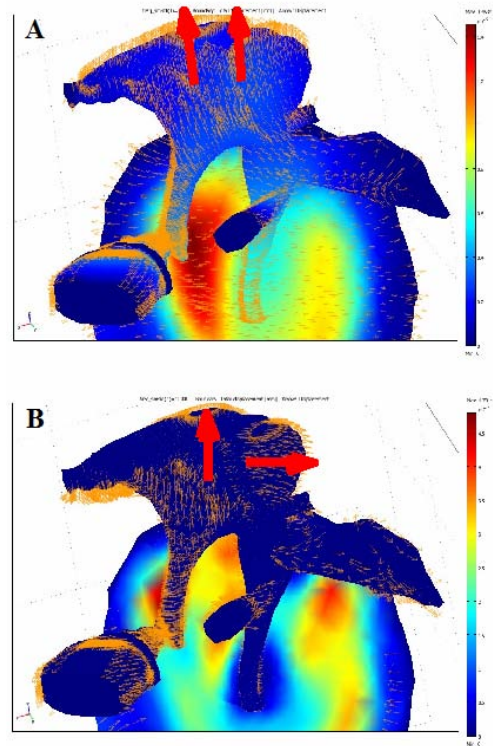
### 3.2 Different motion modes at low and high frequencies

Figure 5 shows different motion modes of ME structures at low and high frequencies at the MIJ complex: Panel A is the displacement field of ME structures at 100 Hz. The two big parallel arrows, which represent the average motion



**Figure 4.** Model  $V_{st}/V_{um}$  curves compared to the corresponding measured data. The  $V_{st}/V_{um}$  experimental data are shown in green circle markers. The upper plot contains unitless velocity ratio amplitudes, while the lower plot contains the phase curves in units of radian/ $\pi$ . Our model fit was plotted in thick blue line, while simulation curves from O'connor and Puria (2008) are shown in red thin dash lines.

direction of the geometric points on Malleus and incus near MIJ, show that malleus and incus rotate about a common axis: the classical hinging motion dominants at low frequencies; Panel B shows the displacement field of ME structures at 10 kHz. The two motion-direction representative arrows are now approximately perpendicular to each other, indicating malleus and incus rotate about two non-parallel axes: a bevel-gear like motion mechanism at high frequencies. Since the displacements in the ossicles are small compare to those in the eardrum, the arrows are normalized and therefore only an indicator of motion directions. Multi-resonance vibration modes at the eardrum were also observed at 10 kHz (Fig. 5).



**Figure 5.** Displacement fields of ME structures at 100 Hz (A) and 10 kHz (B), respectively.

In Figure 5, the displacement fields are a snapshot at the initial time ( $t = 0$ ). Figure 6 shows the average rotation axes of malleus (dash lines) and incus (solid lines) during one motion cycle, computed at 100 Hz (blue lines) and 10 kHz (red lines) respectively. The average rotation axes of malleus and incus at 100 Hz are parallel (hinging motion), while those at 10 kHz are perpendicular to each other (indicative of a bevel-gear like mechanism). Representative eighteen groups of three points on malleus or incus boundaries were used to compute the rotation axes.

Figure 7 shows the angular velocity of malleus (dash lines) and incus (solid lines) around the first (red lines), second (blue lines) and third (green lines) principal axis of the malleus-MIJ-incus complex. At low frequencies, the angular velocities of the malleus and incus are similar (both amplitude and phase), indicating that they rotate approximately around a common axis, while at high frequencies, the angular-velocity amplitude and phase of malleus

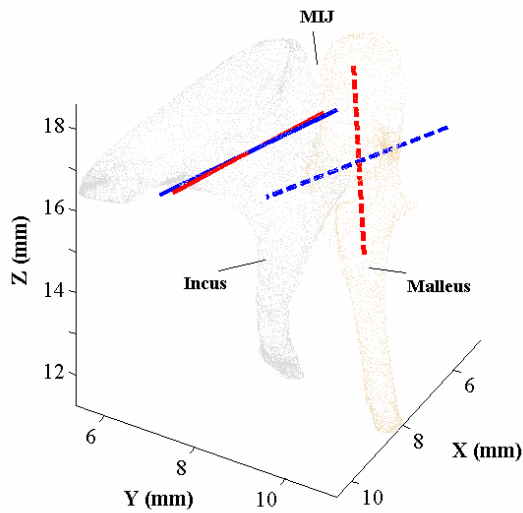


**Figure 6.** Average rotation axes of malleus (dash lines) and incus (solid lines), computed at 100 Hz (blue lines) and 10 kHz (red lines), respectively.

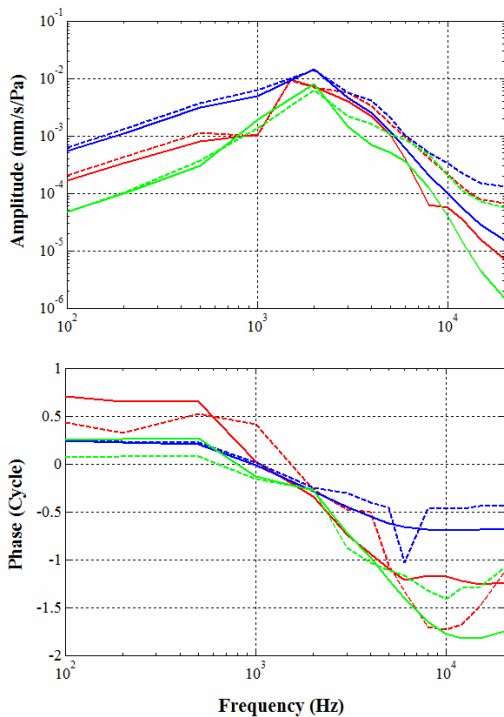


**Figure 7.** Mean angular velocity of malleus (dash lines) and incus (solid lines) around the first (red), second (blue) and third (green) principal axis of the malleus-MIJ-incus complex. The upper plot contains amplitude curves, while the lower plot contains the phase curves.

and incus are relatively different, indicating that they rotate around different axis. We also computed the angular velocities of malleus and incus about the principal frames of malleus and incus, and obtained similar conclusions.

#### 4. Conclusion and Discussion

Mammals' ability to hear high frequency sounds is due to the unique structures in their hearing organ including the three middle ear bones, the shape and connecting mechanism of which are further distinctive in larger mammals like human: cylindrical malleus shape, asymmetric eardrum and mobile saddle-shaped MIJ. These latter unique structural features are favorable to the existence of complex twisting motion at the malleus-incus complex. To test this hypothesis, the motion modes of human middle ear structures were investigated through FE analysis. Our results indicate that at low frequencies, the classical hinging motion is dominant, as expected. However, at high frequencies, we observe a spatial shift in the motion axis of the incus relative to the malleus in order to efficiently drive the stapes. This suggests that the middle ear motion modes and dynamics are determined by the special anatomical features and the three-dimensional inertial properties of the ossicles. The twisting mode of the malleus and incus are required in larger mammals, like humans, in order to reduce the inertia due to ossicular mass. In smaller mammals, like guinea pig and chinchilla, however, the ossicular moment of inertia is small and consequently the gear mechanism is not needed. This leads to different ME structures: I-beam like malleus shape, symmetric eardrum, fused malleus-incus joint (Puria and Steele, 2010).

#### 5. References

1. Aibara, R., Welsh, J. T., Puria, S., and R. L. Goode, Human middle ear sound transfer function and cochlear input impedance, *Hear. Res.*, **152**, 100–109 (2001)
2. Békésy, G., *Experiments in Hearing*, McGraw-Hill, New York (1960)

3. Fay, J. P., Puria, S., and C.R. Steele, The discordant eardrum, *Proc. Natl. Acad. Sci. U.S.A.*, **103**, 19743–19748 (2006)
4. Feng, B., and R.Z. Gan, Lumped parametric model of the human ear for Sound Transmission, *Biomech. Model Mechnobiol.*, **3**, 33-47 (2004)
5. Gan, R., Feng, B. and Q. Sun, Three-dimensional finite element modeling of human ear for sound transmission, *J. Acoust. Soc. Am.*, **32(6)**, 847-859 (2004)
6. Goode, R.L., Killion, M., Nakamura and S. Nishihara, New knowledge about the function of the human middle ear: Development of an improved analog model, *Am. J. Otol.*, **15**, 145-154 (1994)
7. Homma, K., Shimizu, Y. and S. Puria, Ossicular resonance modes of the human middle ear for bone and air conduction, *J. Acoust. Soc. Am.*, **125(2)**, 968-979 (2009)
8. Koike, T., Wada, H., and T. Kobayashi, Modeling of the human middle ear using the finite-element method, *J. Acoust. Soc. Am.*, **111**, 1306–1317 (2002)
9. Kringlebotn, M., Network model for the human middle ear, *Scand. Audiol.*, **17**, 75-85 (1988)
10. O'Conner, K.N. and S. Puria, Middle-ear circuit model parameters based on a population of human ears, *J. Acoust. Soc. Am.*, **123(1)**, 197-211 (2008)
11. Puria, S. and J. B. Allen, A Parametric Study of Cochlear Input Impedance, *J Acoust Soc Am.*, **89**, 287-309 (1991)
12. Puria, S. and C. Steele, Tympanic-membrane and malleus-incus-complex co-adaptations for high-frequency hearing in mammals, *Hear Res.*, **263(1-2)**, 183-190 (2010)
13. Shera, C. A. and G. Zweig, A Symmetry Suppresses the Cochlear Catastrophe, *J Acoust Soc Am.*, **89**, 1276-1289 (1991)
14. Sim, J.H. and S. Puria, Soft Tissue Morphometry of the malleus-incus complex from Micro-CT imaging, *JARO*, **9**, 5-21 (2008)
15. Sim, J. H., Puria, S., and C.R. Steele, Calculation of inertial properties of the malleus-incus complex from micro-CT imaging, *J. Mech. Mater. Struct.*, **2**, 1515–1524 (2007)
16. Wada, H., and T. Metoki, Analysis of dynamic behavior of human middle ear using a finite method, *J. Acoust. Soc. Am.*, **92**, 3157-3168 (1992)
17. Wever, E. G. and M. Lawrence, *Physiological Acoustics*, Princeton University Press, Princeton (1982)

## 6. Acknowledgements

This work was supported by Grant No. R01 DC 005969 and ARRA supplements from the NIDCD of the NIH.